Oxidative stress-mediated hemolytic activity of solvent exchange-prepared fullerene (C-60) nanoparticles

Article *in* Nanotechnology · September 2010

DOI: 10.1088/0957-4484/21/37/375102 · Source: PubMed

CITATIONS
16

READS
182

11 authors, including:

Andreja Trpkovic
Vinča Institute of Nuclear Sciences
16 PUBLICATIONS **262** CITATIONS

SEE PROFILE

Biljana Todorović-Marković
Vinča Institute of Nuclear Sciences
106 PUBLICATIONS **1,667** CITATIONS

SEE PROFILE

Duška N. Kleut
Vinča Institute of Nuclear Sciences
19 PUBLICATIONS **217** CITATIONS

SEE PROFILE

Maja Misirkic Marjanovic
University of Belgrade
30 PUBLICATIONS **785** CITATIONS

SEE PROFILE

Oxidative stress-mediated hemolytic activity of solvent exchange-prepared fullerene (C_{60}) nanoparticles

2010 Nanotechnology 21 375102

(http://iopscience.iop.org/0957-4484/21/37/375102)

Nanotechnology **21** (2010) 375102 (10pp) doi:10.1088/0957-4484/21/37/375102

Oxidative stress-mediated hemolytic activity of solvent exchange-prepared fullerene (C_{60}) nanoparticles

Andreja Trpkovic[1,4], Biljana Todorovic-Markovic[1,4], Duska Kleut[1], Maja Misirkic[2,3], Kristina Janjetovic[2,3], Ljubica Vucicevic[2,3], Aleksandar Pantovic[3], Svetlana Jovanovic[1], Miroslav Dramicanin[1], Zoran Markovic[1,5] and Vladimir Trajkovic[3,5]

[1] Vinca Institute of Nuclear Sciences, POB 522, University of Belgrade, Belgrade 11000, Serbia
[2] Institute for Biological Research 'Sinisa Stankovic', University of Belgrade, Serbia
[3] Institute of Microbiology and Immunology, School of Medicine, University of Belgrade, Dr Subotica 1, Belgrade 11000, Serbia

E-mail: zormark@vinca.rs and vtrajkovic@eunet.rs

Received 31 May 2010, in final form 23 July 2010
Published 20 August 2010
Online at stacks.iop.org/Nano/21/375102

Abstract

The present study investigated the hemolytic properties of fullerene (C_{60}) nanoparticles prepared by solvent exchange using tetrahydrofuran (nC_{60}THF), or by mechanochemically assisted complexation with macrocyclic oligosaccharide gamma-cyclodextrin (nC_{60}CDX) or the copolymer ethylene vinyl acetate–ethylene vinyl versatate (nC_{60}EVA–EVV). The spectrophotometrical analysis of hemoglobin release revealed that only nC_{60}THF, but not nC_{60}CDX or nC_{60}EVA–EVV, was able to cause lysis of human erythrocytes in a dose- and time-dependent manner. Atomic force microscopy revealed that nC_{60}THF-mediated hemolysis was preceded by erythrocyte shrinkage and increase in cell surface roughness. A flow cytometric analysis confirmed a decrease in erythrocyte size and demonstrated a significant increase in reactive oxygen species production in red blood cells exposed to nC_{60}THF. The nC_{60}THF-triggered hemolytic activity was efficiently reduced by the antioxidants *N*-acetylcysteine and butylated hydroxyanisole, as well as by serum albumin, the most abundant protein in human blood plasma. These data indicate that nC_{60}THF can cause serum albumin-preventable hemolysis through oxidative stress-mediated damage of the erythrocyte membrane.

(Some figures in this article are in colour only in the electronic version)

1. Introduction

Because of the unique chemical and physical properties that enable interaction with living cells, the C_{60} fullerene has recently gained considerable attention as a promising candidate for various biomedical applications. Many fullerene-based compounds targeting different biological molecules have been synthesized, displaying a range of biological activities potentially useful in anticancer or antimicrobial therapy, cytoprotection, enzyme inhibition, controlled drug delivery and diagnostic imaging [1–3]. Since the C_{60} is virtually insoluble in water, several solubilization procedures have been devised, including chemical modification by attachment of different functional groups, complexation with water-soluble host molecules, or the solubilization in organic solvents followed by the solvent replacement with water (solvent exchange), which all produce water suspensions of fullerene nanoparticles [4, 5]. However, C_{60} nanoparticles produced by different solubilization methods display profoundly distinct biological activities. For example, while all photo-irradiated

[4] These authors equally contributed to the work.
[5] Authors to whom any correspondence should be addressed.

C_{60} nanoparticles produce reactive oxygen species (ROS) as important cell-signaling and cytotoxic agents, non-irradiated fullerene preparations markedly differ in this respect [5]. Namely, it has been shown that in the absence of irradiation, water-soluble C_{60} derivatives and complexes with different host molecules protect cells by quenching cytotoxic ROS [6–11], while C_{60} nanoparticles prepared by solvent exchange using tetrahydrofuran produce large amounts of ROS and kill cells by inducing oxidative stress [12–15].

Although a high degree of blood compatibility is an obvious prerequisite for the biomedical applications of C_{60}, only few studies thus far have examined the hemolytic activity of fullerene nanoparticles. It has been reported that bis-methanophosphonate-C_{60}, mono-methanophosphonic acid-C_{60} and dimalonic acid-C_{60} were all able to cause ROS-mediated damage to erythrocyte membrane upon photo-irradiation [16]. In another study performed in the absence of intentional photo-irradiation, water-soluble C_{60} derivatives with cationic chains attached to the carbon cage were highly hemolytic, while the presence of neutral or anionic moieties did not affect erythrocyte integrity [17]. The surfactant properties of the cationic fullerene derivatives, generated by a simultaneous presence of hydrophobic and hydrophilic portions, were proposed to be responsible for the erythrocyte membrane disruption [17]. To the best of our knowledge, the hemolytic activity of chemically non-modified fullerenes has not been tested thus far.

The aim of this study was to investigate the possible hemolytic activity of chemically non-modified fullerene nanoparticles produced by solvent exchange and encapsulation in water-soluble host molecules. We demonstrate that C_{60} nanoparticles prepared by solvent exchange using tetrahydrofuran, but not those produced by complexation with macrocyclic oligosaccharide γ-cyclodextrin or the copolymer ethylene vinyl acetate–ethylene vinyl versatate, cause oxidative stress-mediated lysis of human red blood cells (RBC).

2. Materials and methods

2.1. Materials

C_{60} (99.9% purity) was obtained from Bucky USA (Houston, TX). Tetrahydrofuran (99.99%), phosphate-buffered saline, γ-cyclodextrin, *N*-acetylcysteine, butylated hydroxyanisole and bovine serum albumin (BSA) were from Sigma-Aldrich (St Louis, MO). Ethylene vinyl acetate–ethylene vinyl versatate was kindly provided by Celanese GMBH (Frankfurt, Germany). Dihydrorhodamine (DHR) and 2′,7′-dichlorodihydrofluorescein diacetate (DCFDA) were purchased from Invitrogen (Carlsbad, CA).

2.2. Preparation of fullerene nanoparticles

The water suspensions of fullerene nanoparticles were prepared by solvent exchange, using tetrahydrofuran (THF) to initially dissolve C_{60} ($nC_{60\text{THF}}$) [18], or by mechanochemically assisted complexation with macrocyclic oligosaccharide gamma-cyclodextrin ($nC_{60\text{CDX}}$) or the copolymer ethylene vinyl acetate–ethylene vinyl versatate ($nC_{60\text{EVA–EVV}}$) [10]. The C_{60} nanoparticles were characterized by UV–vis, dynamic light scattering (DLS), and atomic force microscopy (AFM) as previously described [10, 18]. The ultraviolet absorption spectra of all three fullerene suspensions showed characteristic peaks around 270 and 340 nm (figure 1(A)). The average size of nanoparticles determined by DLS was approximately 100 nm ($nC_{60\text{THF}}$), 125 nm ($nC_{60\text{CDX}}$) and 55 nm ($nC_{60\text{EVA–EVV}}$), with relatively uniform particle size distribution (figure 1(B)). The representative AFM images are presented in figure 1(C). Immediately before the experiments, 10× phosphate-buffered saline (PBS) was used to prepare the fullerene suspensions in PBS (10 μg ml^{-1} $nC_{60\text{THF}}$, 100 μg ml^{-1} $nC_{60\text{CDX}}$ and 100 μg ml^{-1} $nC_{60\text{EVA–EVV}}$).

2.3. RBC preparation and determination of fullerene hemolytic activity

The research has been approved by our institutional ethics committee and performed in accordance with the ethical standards of the 1964 declaration of Helsinki. Blood of the volunteers, who all gave informed consent, was collected in 5 ml ethylenediaminetetraacetate-containing vacutainers and erythrocyte hemolysis was determined spectrophotometrically as previously described [19]. Briefly, after blood sedimentation by centrifugation (1000*g*, 3 min, 4 °C), plasma, platelets and leukocytes were removed by pipetting and erythrocytes were washed three times in 0.9% NaCl. The RBC suspension was finally diluted with freshly prepared phosphate-buffered saline (PBS; 150 mM, pH 7.4) to obtain a suspension containing 10^7 RBC ml^{-1}. To assess the fullerene hemolytic activity, 100 μl of fullerene suspension in PBS was added to 900 μl of RBC suspension, mixed by inversion and incubated for 1, 6, or 18 h at 37 °C in a humidified atmosphere with 5% CO_2. In some experiments, bovine serum albumin or antioxidants *N*-acetylcysteine and butylated hydroxyanisole were used in addition to fullerenes, as described in results and/or figure captions. After each hour of the first six hours of incubation, the samples were mixed by inversion. At the end of incubation, the samples were centrifuged (1000*g*, 3 min, 4 °C), the supernatants were removed and analyzed for hemoglobin content by spectrophotometric measurement of absorbance at 540 nm. The degree of hemolysis was calculated as the hemolytic index:

$$\%\text{H} = (A_\text{s} - A_\text{nc} - A_0)100/A_\text{pc}$$

where A_s is the absorbance of the sample, A_nc the absorbance of the negative control containing only the fullerenes in PBS, A_0 the absorbance of RBC suspension in PBS, and A_pc the absorbance of the positive control (RBC completely lysed in deionized water).

2.4. Flow cytometry analysis of RBC morphology and intracellular ROS production

Flow cytometry analysis was performed on a FACSCalibur flow cytometer (BD Biosciences, Heidelberg, Germany), using CellQuest Pro software for acquisition and analysis.

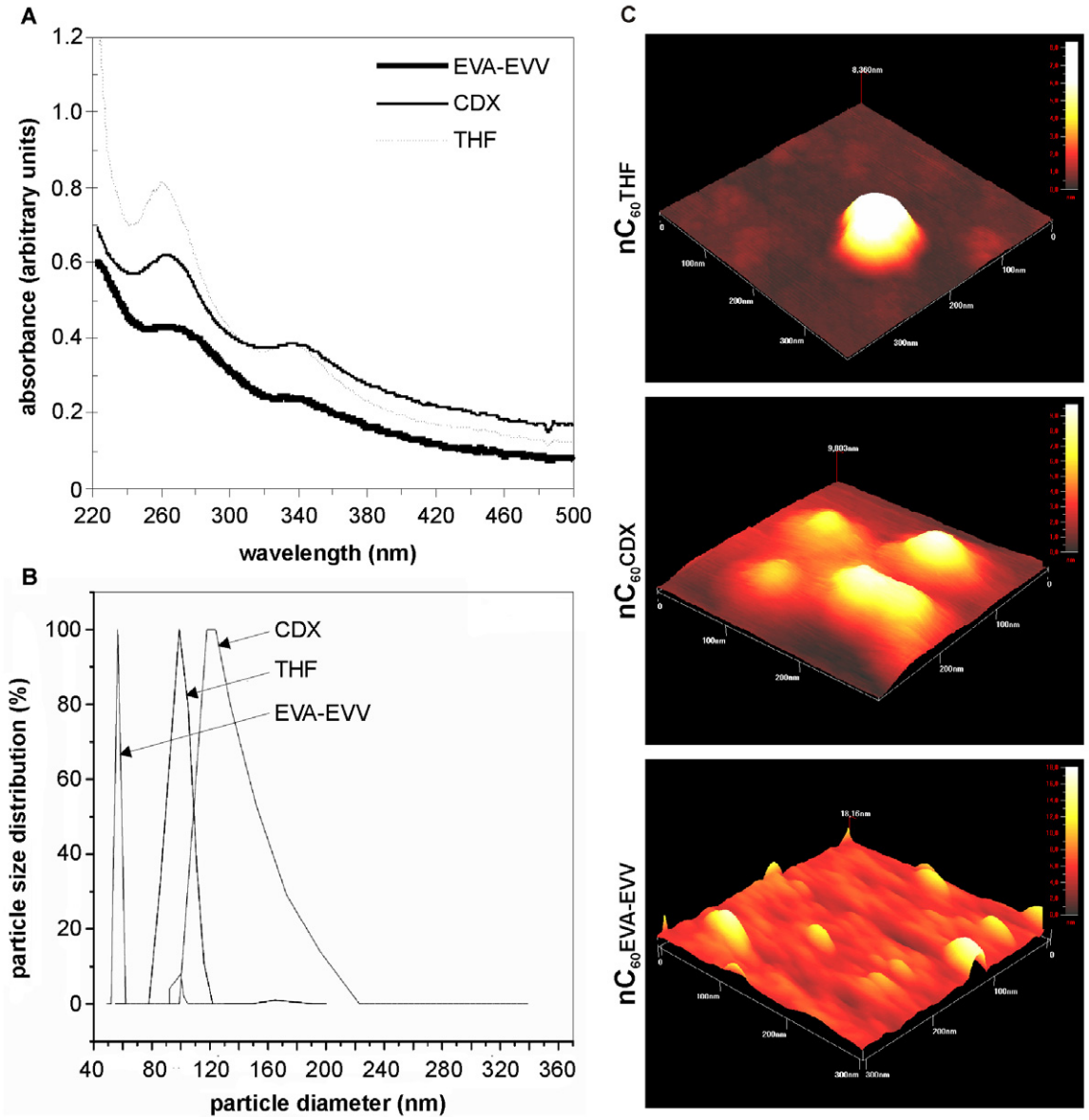

Figure 1. Characterization of C_{60} nanoparticles. (A) UV–vis showing C_{60} characteristic peaks (270 and 340 nm). (B) Normalized size distribution of C_{60} nanoparticles. (C) Representative AFM images of C_{60} nanoparticles.

The light-scatter channels were set on linear gains and the fluorescence channels on a logarithmic scale. A minimum of 10 000 cells were analyzed in each condition, adjusting the threshold settings so that the cell debris and large nanoparticle aggregates were excluded from the data acquisition. Erythrocyte size and density were assessed using forward scatter (FSC) and side scatter (SSC), respectively. The intracellular production of ROS was determined by measuring the intensity of green fluorescence emitted by redox-sensitive dyes dihydrorhodamine 123 (DHR) or 2′,7′-dichlorofluorescein diacetate (DCFDA). DHR (2 μM) or DCFDA (10 μM) were added to RBC suspensions 10 min prior to treatment with C_{60} nanoparticles. At the end of incubation, the RBC were washed in PBS and the geomean intensity of the green fluorescence (FL1), corresponding to ROS production, was determined.

2.5. AFM analysis of RBC morphology

After treatment with nC$_{60}$THF for 15, 30 and 60 min, 10 μl of RBC suspension was dropped on the freshly cleaned glass surface, fixed with methanol and then air-dried. AFM (Quesant, Santa Cruz, CA) was performed in the tapping mode in air. The sample was mounted onto the XY stage of the AFM and the integral video camera was used to locate and relocate the regions of interest when the different tips were changed. The curvature radius of the silicon tip was less than 10 nm, while for the tips used in the tapping mode, the length of cantilever was 125 μm, the oscillation frequency was 136 kHz, and the force constant was 10 N m^{-1}. The scan rate was 0.3–1 Hz and the scanning range of the closed-loop scanner was 35 μm. All acquired images (256 pixels × 256 pixels) were processed with the instrument-equipped software to

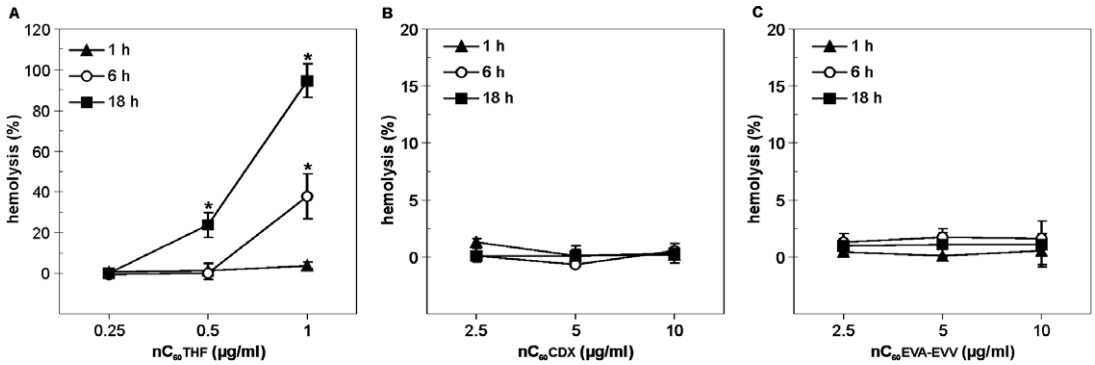

Figure 2. Hemolytic effect of nC$_{60}$THF. Red blood cells (RBC) were incubated without or with different concentrations of nC$_{60}$THF (A), nC$_{60}$CDX (B) or nC$_{60}$EVA–EVV (C), and hemolysis was determined spectrophotometrically after 1, 6 or 18 h. The data are mean ± SD values obtained from three different donors ($^*p < 0.05$ refers to untreated cells with 0% hemolysis).

level the images and presented in the wave mode unless stated otherwise. The root-mean-square value of the surface roughness ($R_{\rm rms}$) was calculated according to the formula:

$$R_{\rm rms} = \sqrt{\left[\sum_{n=1}^{N}(z_n - z_{\rm av})^2\right]}$$

where N represents the total number of data points in a selected area, z_n is the height of the nth point, and $z_{\rm av}$ is the average height. The roughness was directly generated by the Quesant software.

2.6. Statistics

The statistical significance of the differences was analyzed by t-test or one-way ANOVA followed by the Student–Newman–Keuls test. The value of $p < 0.05$ was considered significant.

3. Results

3.1. Hemolytic activity of different C_{60} nanoparticles

The hemolytic potentials of nC$_{60}$THF, nC$_{60}$CDX and C$_{60}$EVA–EVV were assessed by incubating fullerene nanoparticles with human RBC for 1, 6 and 18 h, followed by colorimetric analysis of the released hemoglobin. The nC$_{60}$THF (0.25–1 μg ml^{-1}) displayed a significant dose- and time-dependent hemolytic activity, with 0.5 μg ml^{-1} causing hemolysis only at 18 h, and 1 μg ml^{-1} both at 6 and 18 h of treatment (figure 2(A)). On the other hand, neither nC$_{60}$CDX nor nC$_{60}$EVA–EVV at ten-fold higher concentrations (2.5–10 μg ml^{-1}) were toxic to erythrocytes during 18 h of incubation (figures 2(B) and (C)). It therefore appears that nC$_{60}$THF, but not nC$_{60}$CDX or nC$_{60}$EVA–EVV, was able to cause lysis of human RBC. The observed hemolysis was not due to a direct toxicity of residual THF (<10% w/w) intercalated in nC$_{60}$THF crystalline lattice [13], as THF alone was not hemolytic after 18 h even at concentrations 100-fold higher (10 μg ml^{-1}) than its estimated residual presence (<0.1 μg ml^{-1}) in 1 μg ml^{-1} solution of nC$_{60}$THF (data not shown).

3.2. Morphological changes induced by nC$_{60}$THF treatment of RBC

Next, flow cytometry and AFM were employed to evaluate the changes in erythrocyte morphology upon treatment with nC$_{60}$THF (1 μg ml^{-1}). The analysis of flow cytometry dot plots (figure 3(A)), histograms (figure 3(B)) and geometric mean fluorescence (figure 3(C)) revealed that 1 h treatment of RBC with nC$_{60}$THF reduced both FSC and SSC values in comparison with untreated cells, thus indicating a decrease in size (FSC) and density (SSC) of erythrocytes. This was confirmed by AFM investigation, which demonstrated a significant reduction in both diameter and height of RBC exposed to nC$_{60}$THF for 30 or 60 min (figure 4). In addition, the AFM analysis has shown that the surface of erythrocytes became scalloped/notched after 30 min of treatment with nC$_{60}$THF (figure 4(A)), which was accordingly reflected in a significant increase in $R_{\rm rms}$ surface roughness value (figure 4(B)). After 60 min, more prominent defects in erythrocyte morphology corresponding to a further increase in surface roughness were observed (figures 4(A) and B). Therefore, nC$_{60}$THF treatment caused RBC shrinkage with subsequent crenation and loss of a typical discoid shape. We did not observe any significant morphological changes detectable by flow cytometry or AFM in erythrocytes treated with 10 μg ml^{-1} of nC$_{60}$CDX or C$_{60}$EVA–EVV (data not shown).

3.3. The role of oxidative stress in nC$_{60}$THF-mediated hemolysis

A flow cytometric analysis was used to assess the influence of nC$_{60}$THF on intracellular production of ROS in human erythrocytes. The fluorescence of redox-sensitive dyes DHR and DCFDA markedly increased in RBC exposed to nC$_{60}$THF (1 μg ml^{-1}) for 1 h, indicating an increase in intraerythrocytic generation of ROS (figures 5(A) and (B)). No significant increase in DHR or DCFDA fluorescence was observed upon RBC treatment with 10 μg ml^{-1} of nC$_{60}$CDX or C$_{60}$EVA–EVV (data not shown). To evaluate the involvement of oxidative stress in nC$_{60}$THF-mediated hemolysis, we used the well-known antioxidant agents N-acetylcysteine (4 and 8 mM) and butylated hydroxyanisole (100 and 200 μM). Both antioxidants reduced the hemolytic effect of nC$_{60}$THF in a

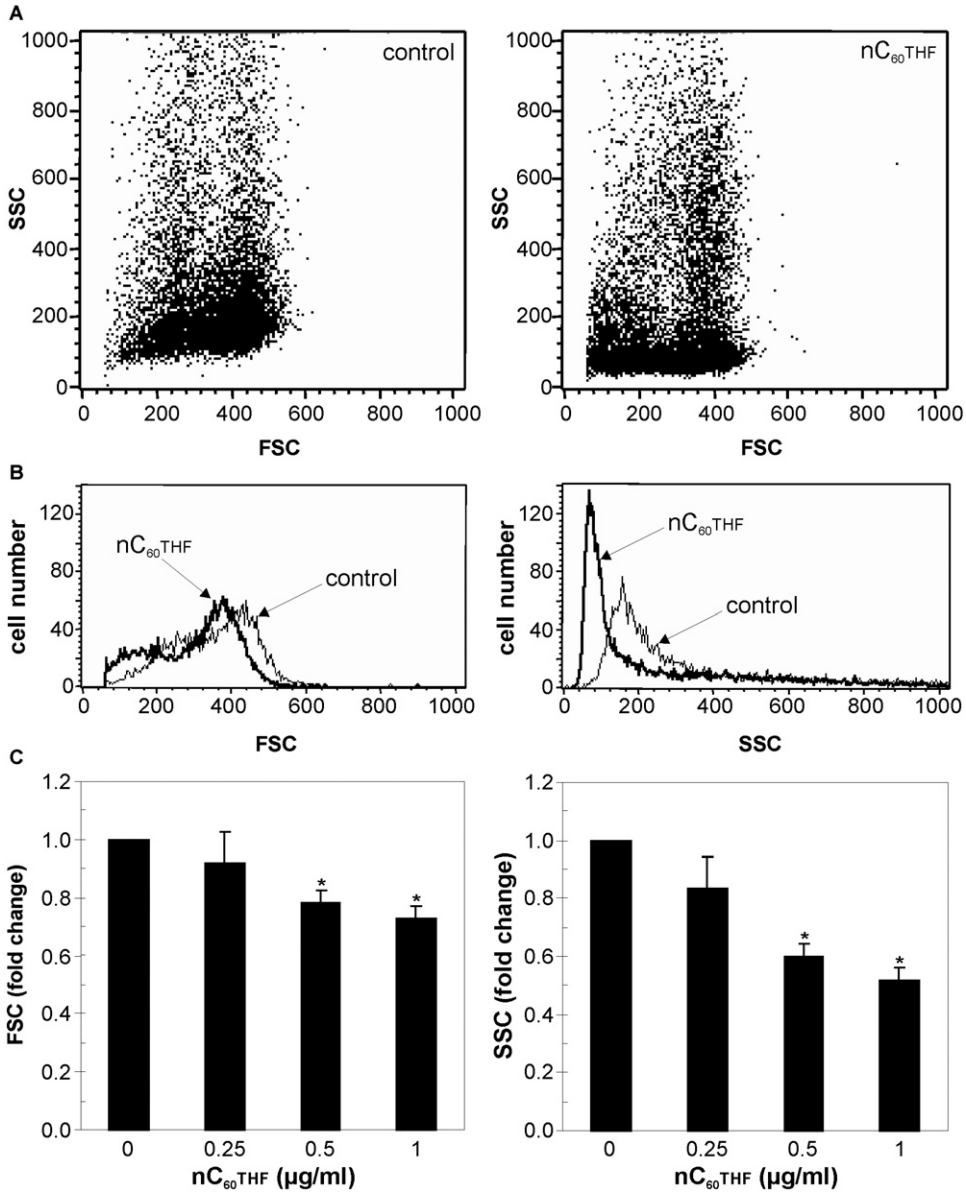

Figure 3. Flow cytometry analysis of nC$_{60}$THF-induced changes in RBC morphology. Erythrocytes were incubated without or with 1 μg ml^{-1} ((A), (B)) or different concentrations (C) of nC$_{60}$THF for 1 h and FSC/SSC values were determined by flow cytometry. Representative dot plots and histograms are presented in (A) and (B), respectively, while the mean $\pm$ SD values of FSC/SSC geomean fluorescence obtained from three different donors are presented in (C) ($^{*}p < 0.05$ refers to untreated cells).

dose-dependent manner (figure 5(C)), thus confirming that the observed hemotoxicity was at least partly dependent on the induction of oxidative stress.

3.4. Inhibition of nC$_{60}$THF-mediated hemolysis by serum albumin

We finally investigated if serum albumin, as the most abundant protein in human blood plasma, could affect the hemotoxic effect of fullerene nanoparticles. Indeed, the hemolytic activity of nC$_{60}$THF (1 μg ml^{-1}) was significantly reduced if it was mixed with BSA at the concentration present in blood (40 mg ml^{-1}) 1 h prior to incubation with erythrocytes (figure 6(A)). To assess if nC$_{60}$THF makes complexes with albumin, we heat-precipitated BSA from the mixture of nC$_{60}$THF (10 μg ml^{-1}) and BSA (40 mg ml^{-1}) at 95 °C, as previously described [20]. The control sample containing only nC$_{60}$THF was subjected to the same procedure. The samples were centrifuged at 6000 rpm for 30 min, supernatant was removed and investigated by UV–vis for the presence of nC$_{60}$THF. As it can be seen from the UV–vis spectra in figure 6(B), C$_{60}$ absorption bands (270 and 340 nm) were clearly evident in the supernatant of the control nC$_{60}$THF sample, but barely visible in the supernatant of the nC$_{60}$THF/BSA mixture, thus indicating an interaction of nC$_{60}$THF with albumin. To get some insight into the morphology of nC$_{60}$THF/BSA complexes, we performed AFM analysis of particles in the nC$_{60}$THF/BSA mixture (1 μg ml^{-1} +

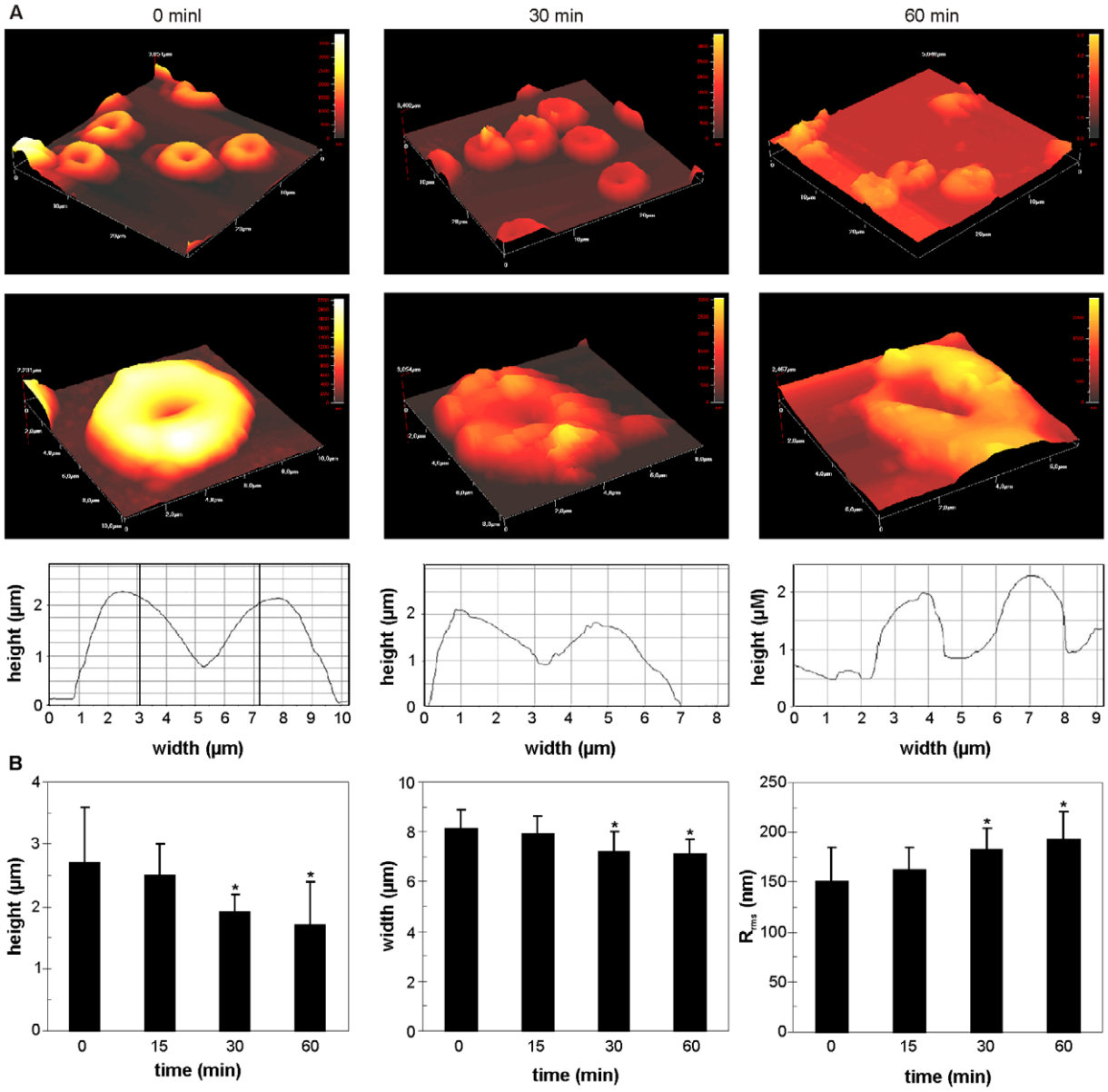

Figure 4. AFM analysis of nC$_{60}$THF-induced changes in RBC morphology. ((A), (B)) Erythrocytes were incubated with nC$_{60}$THF (1 μg ml^{-1}) for the indicated time periods and the cell width, height and surface roughness were examined by AFM. Representative AFM images and corresponding width/height plots are presented in (A), while the mean $\pm$ SD values of height, width and surface roughness (R_{rms}) are presented in (B) ($^*p < 0.05$ refers to untreated cells; $n = 10$).

5 μg ml^{-1}) in both wave mode and phase mode. A number of particles in the mixture had irregular shape and were larger (approx. 200 nm) than nC$_{60}$THF (100 nm; figure 1(C)) or albumin particles (20 nm; figure 6(C), top), as shown in the representative AFM wave mode image (figure 6(C), middle), indicating that nC$_{60}$THF/albumin complexes were formed. We next used the ability of the phase mode to distinguish between different materials in a sample, with the direction of the phase change depending on the nature of the interaction between the probe and the surface. If the particle is homogeneous, the phase shift of the cantilever remains constant as the probe is rastered across the sample and the phase image displays a uniform flat image of constant phase. However, the phase mode image shown in figure 6(C) (bottom) is consistent with the composite nature of the particle, with the rim probably composed of aggregated smaller albumin particles and interacting with the probe more intensely than the central part which presumably contains larger nC$_{60}$THF. Collectively, these data suggest that the expected hemotoxicity of nC$_{60}$THF could be attenuated by complexation with blood albumin.

4. Discussion

The present study shows that C$_{60}$ nanoparticles prepared by solvent exchange method (nC$_{60}$THF) caused shrinkage, crenation and, eventually, hemolysis of human RBC. The erythrocyte damage by nC$_{60}$THF was mediated by oxidative stress and prevented by serum albumin. While

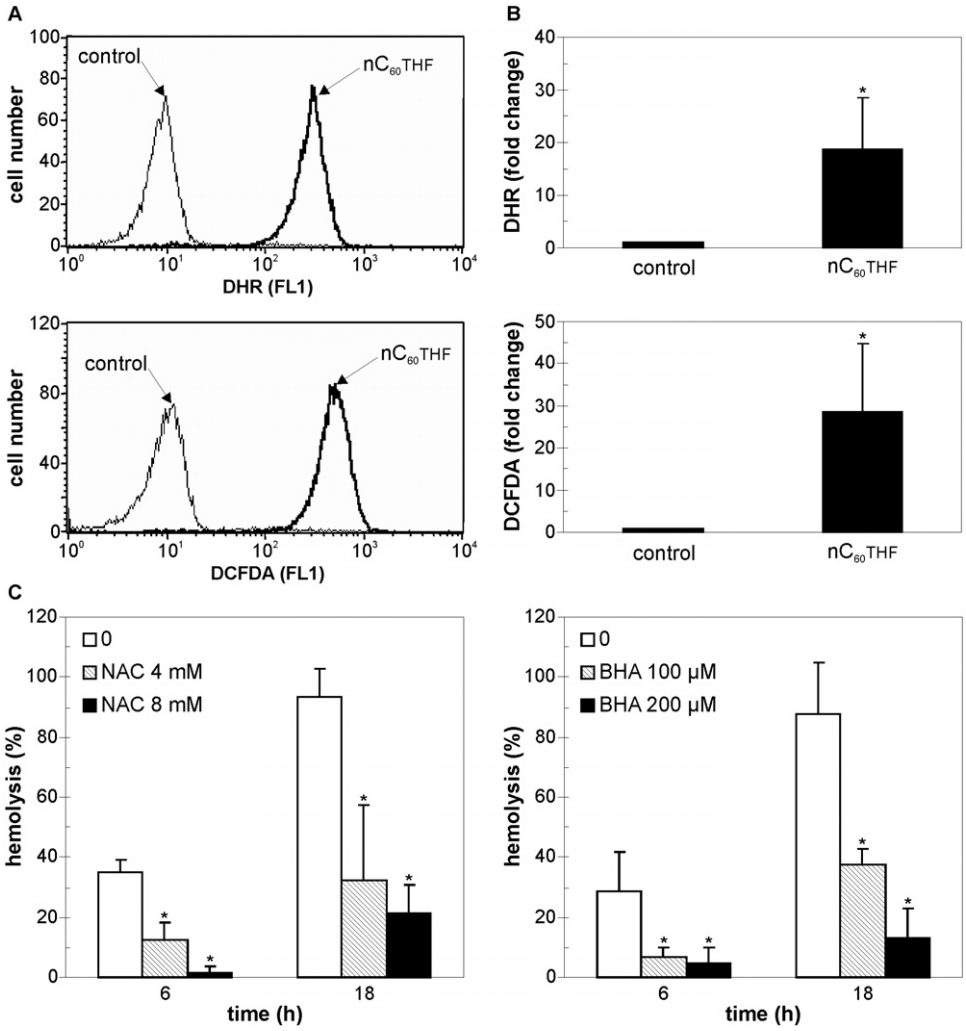

Figure 5. The role of oxidative stress in nC$_{60}$THF-triggered hemolysis. ((A), (B)) Erythrocytes were incubated with nC$_{60}$THF (1 μg ml^{-1}) for 1 h and ROS production was examined in DHR- or DCFDA-stained cells by flow cytometry. Representative histograms are presented in (A), while the mean $\pm$ SD fluorescence values obtained from three different donors are presented in (B) ($^{*}p < 0.05$ refers to untreated cells). (C) Erythrocytes were incubated with nC$_{60}$THF (1 μg ml^{-1}) in the absence or presence of different concentrations of antioxidants *N*-acetylcysteine (NAC) or butylated hydroxyanisole (BHA) and hemolysis was assessed after 6 and 18 h ($^{*}p < 0.05$ refers to cells treated with nC$_{60}$THF alone).

the hemolytic activity of both photo-irradiated and non-irradiated water-soluble fullerene derivatives has previously been reported [16, 17], this is, to the best of our knowledge, the first report describing the hemolytic properties of chemically non-modified fullerenes.

In contrast to nC$_{60}$THF, the C$_{60}$ nanoparticles prepared by complexation with gamma-cyclodextrin (nC$_{60}$CDX) or vinyl acetate–ethylene vinyl versatate (nC$_{60}$EVA–EVV) did not display significant hemolytic effect. Since the average size of nC$_{60}$THF was between that of nC$_{60}$EVA–EVV and nC$_{60}$CDX, it seems unlikely that the different surface-to-volume ratios of fullerene nanoparticles contributed to the difference in their hemolytic activity. A more plausible explanation for this discrepancy is that nC$_{60}$THF, but not nC$_{60}$CDX or nC$_{60}$EVA–EVV, can produce high amounts of potentially cell-damaging ROS in the absence of intentional photo-irradiation [10, 12, 13, 15, 18]. Although the mechanisms underlying this unusual property of nC$_{60}$THF are not completely elucidated, the available data suggest the involvement of the interaction between C$_{60}$ and residual THF that remains intercalated into the nano-C$_{60}$ crystalline lattice [18, 21, 22]. Such a hypothesis is consistent with the present finding that THF alone failed to reproduce the effects of nC$_{60}$THF on erythrocytes. It should be noted that we did not directly assess the fullerene uptake by RBC, so it could not be confirmed if ROS detected within RBC were actually produced intracelullarly by ingested nC$_{60}$THF, or extracellularly by nC$_{60}$THF in the vicinity of RBC or adsorbed to their membrane. Also, the possibility that the differences in zeta potential might influence the stability of nanoparticles and their interaction with erythrocytes, therefore contributing to their cytotoxicity, is currently being investigated in our laboratory.

Apoptosis and necrosis are two major, morphologically different types of cell demise, generally corresponding to 'programmed' and 'accidental' cell death, respectively [23]. It has recently been described that oxidative stress can induce eryptosis, an apoptosis-like death of erythrocytes,

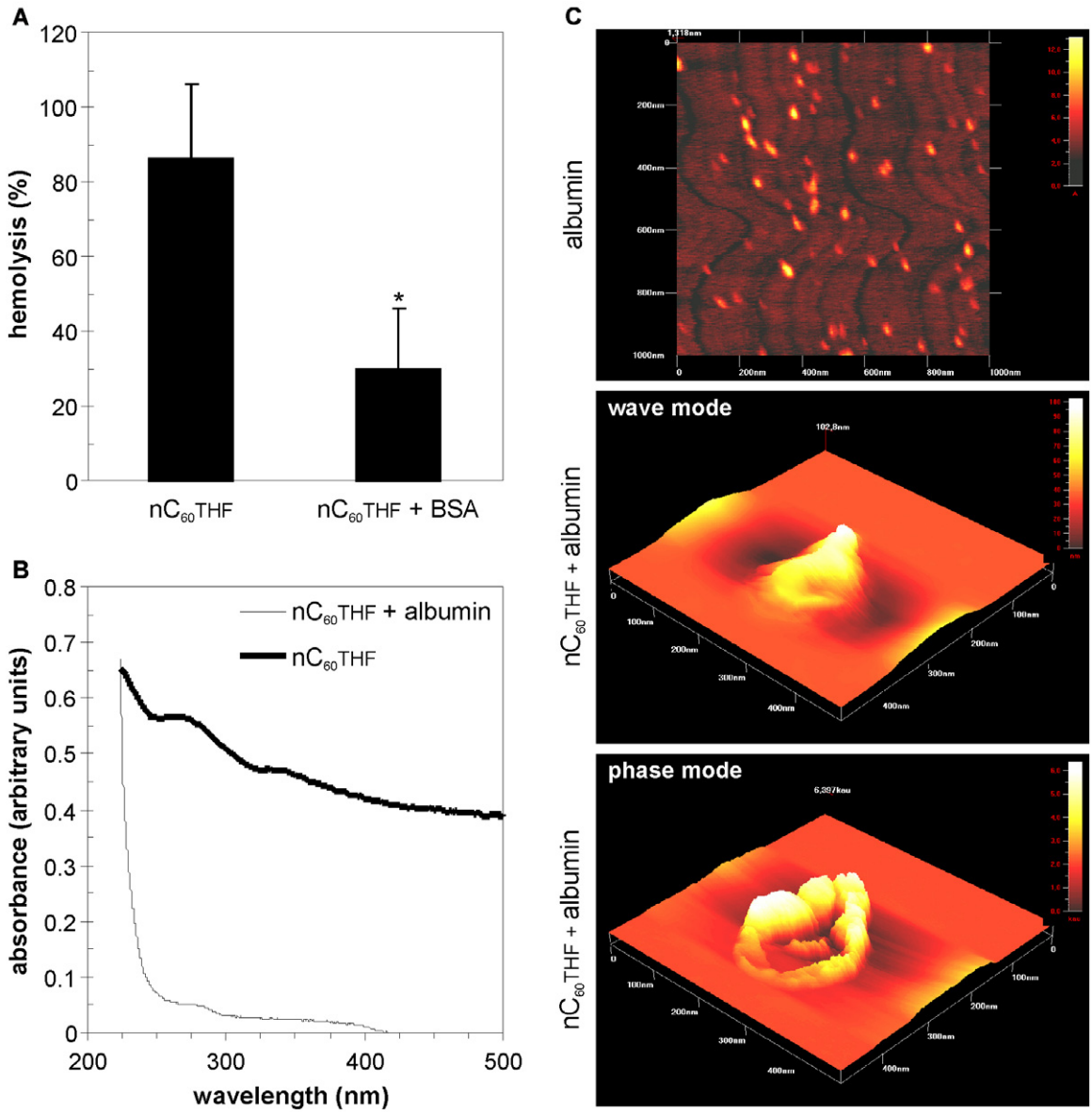

Figure 6. Serum albumin adsorbs to nC$_{60}$THF and reduces its hemotoxicity. (A) Erythrocytes were incubated with nC$_{60}$THF (1 μg ml^{-1}) alone, or with nC$_{60}$THF that was preincubated with BSA (40 mg ml^{-1}) for 1 h before RBC treatment. Hemolysis was assessed after 24 h ($^{*}p < 0.05$). (B) After 1 h co-incubation of BSA (40 mg ml^{-1}) and nC$_{60}$THF (10 μg ml^{-1}), BSA was heat-precipitated and the supernatant was analyzed by UV–vis. The same treatment was applied to control the suspension containing only nC$_{60}$THF. (C) BSA (5 μg ml^{-1}) alone or co-incubated for 1 h with nC$_{60}$THF (5 μg ml^{-1}) was spin-coated on freshly cleaved mica and analyzed by AFM. Both wave mode (middle panel) and phase mode (bottom panel) AFM images of BSA/nC$_{60}$THF mixture are presented.

characterized by decrease in cell volume and cell membrane blebbing [24, 25]. Oxidative stress triggered eryptosis by activation of Ca^{2+}-permeable cation channels and subsequent increase in cytosolic Ca^{2+} concentration [26, 27]. However, the RBC buffer in our study did not contain Ca^{2+}, so it seems safe to conclude that Ca^{2+}-dependent eryptosis was not responsible for the shrinkage and crenation of RBC treated with nC$_{60}$THF. Another possibility is that nC$_{60}$THF caused a necrosis-like erythrocyte damage by increasing the cell membrane permeability through peroxidation of the lipid bilayer, as previously reported for other cell types, including fibroblasts, astrocytes and various types of cancer cells [13, 15, 18, 28]. Indeed, our flow cytometry data are consistent with such an assumption, as necrosis is accompanied by an early decrease in both FSC and SSC values, while an early decrease in FSC during apoptosis is often accompanied by simultaneous increase in SSC [29]. The reduced ability of a necrotic cell to scatter light simultaneously in the forward (FSC) and right angle directions (SSC) probably occurs as a consequence of plasma membrane rupture and leakage of the intracellular content. One should, however, keep in mind that the general rules for FSC/SSC alterations during cell death might not apply for erythrocytes. Also, it is plausible to assume that SSC values will show an early increase due to nanoparticle uptake, which we have actually seen previously with nC$_{60}$CDX and nC$_{60}$EVA–EVV [10], but

not with nC$_{60}$THF in the present study. While the absence of an early SSC increase might indicate that nC$_{60}$THF is not internalized by erythrocytes, this needs to be confirmed by more specific methods for determination of nanoparticle uptake. With these issues remaining to be resolved, we propose the following sequence of events: nC$_{60}$THF, having a high affinity towards cell surface [12, 13], binds the erythrocyte membrane and causes lipid peroxidation-mediated damage by releasing ROS. The ensuing osmotic imbalance leads to erythrocyte dehydration, causing a reduction in cell size and subsequent AMF-detectable crenation due to the protruding membrane-bound spectrin/actin cytoskeleton. As the membrane damage progresses with time, the leakage of hemoglobin and other cellular constituents occurs, eventually manifesting as profound deformations of the erythrocyte shape and hemolysis. Also, the possibility that the accumulation of fullerene nanoparticles at the erythrocyte membrane could contribute to the increase in RBC surface roughness requires further investigation with appropriate analytical techniques (e.g. Raman spectroscopy).

An obvious weakness of the present study is the reductionist approach, which, by neglecting the possible interference of various blood constituents, clearly oversimplifies the interaction of nC$_{60}$THF and RBC in the *in vivo* conditions. In an attempt to partly overcome this drawback, we tested the influence of serum albumin, which comprises about half of the blood serum protein, on the hemolytic activity of nC$_{60}$THF. Our finding that serum albumin markedly attenuated nC$_{60}$THF-induced hemolysis is consistent with its ability to adsorb onto the surface of C$_{60}$ nanoparticles, described previously [30, 31] and confirmed in the present study. In this way, albumin could prevent nC$_{60}$THF interaction with erythrocytes and subsequent damage of their membrane. While it is difficult to extrapolate these findings to the *in vivo* situation, it nevertheless seems plausible to assume that the blood compatibility of intravenously injected nC$_{60}$THF could be significantly improved by subsequent complexation with serum albumin.

In conclusion, we here demonstrate that the hemolytic activity of different preparations of chemically non-modified fullerenes correlates with their ability to release ROS. Our data suggest that fullerene complexes with non-toxic host molecules such as γ-cyclodextrin or EVA–EVV, because of the superior blood compatibility, could be better candidates for *in vivo* biomedical applications than hemolytic nC$_{60}$THF or water-soluble cationic C$_{60}$ derivatives. Nevertheless, further studies, both *in vitro* and *in vivo*, are required to provide new insights into the mechanisms and biological consequences of erythrocyte interaction with different fullerene preparations.

Acknowledgments

This work was supported by the Ministry of Science and Technological Development of the Republic of Serbia (grant No. 145073). The authors thank Dr Ljubica Harhaji-Trajkovic for critically perusing the manuscript.

References

[1] Partha R Conyers J L 2009 biomedical applications of functionalized fullerene-based nanomaterials *Int. J. Nanomed.* **4** 261–75
[2] Bakry R *et al* 2007 Medicinal applications of fullerenes *Int. J. Nanomed.* **2** 639–49
[3] Bosi S, Da Ros T, Spalluto G and Prato M 2003 Fullerene derivatives: an attractive tool for biological applications *Eur. J. Med. Chem.* **38** 913–23
[4] Nakamura E and Isobe H 2003 Functionalized fullerenes in water. The first 10 years of their chemistry, biology, and nanoscience *Acc. Chem. Res.* **36** 807–15
[5] Markovic Z and Trajkovic V 2008 Biomedical potential of the reactive oxygen species generation and quenching by fullerenes (C$_{60}$) *Biomaterials* **29** 3561–73
[6] Dugan L L, Gabrielsen J K, Yu S P, Lin T S and Choi D W 1996 Buckminsterfullerenol free radical scavengers reduce excitotoxic and apoptotic death of cultured cortical neurons *Neurobiol. Dis.* **3** 129–35
[7] Dugan L L *et al* 1997 Carboxyfullerenes as neuroprotective agents *Proc. Natl Acad. Sci. USA* **94** 9434–9
[8] Bisaglia M *et al* 2000 C3-fullero-tris-methanodicarboxylic acid protects cerebellar granule cells from apoptosis *J. Neurochem.* **74** 1197–204
[9] Harhaji L *et al* 2008 Modulation of tumor necrosis factor-mediated cell death by fullerenes *Pharm. Res.* **25** 1365–76
[10] Misirkic M S *et al* 2009 The protection of cells from nitric oxide-mediated apoptotic death by mechanochemically synthesized fullerene (C$_{60}$) nanoparticles *Biomaterials* **30** 2319–28
[11] Lao F *et al* 2009 Fullerene derivatives protect endothelial cells against NO-induced damage *Nanotechnology* **20** 225103
[12] Sayes C M *et al* 2004 The differential cytotoxicity of water-soluble fullerenes *Nano Lett.* **4** 1881–7
[13] Sayes C M, Gobin A M, Ausman K D, Mendez J, West J L and Colvin V L 2005 Nano-C$_{60}$ cytotoxicity is due to lipid peroxidation *Biomaterials* **26** 7587–95
[14] Oberdorster E 2004 Manufactured nanomaterials (fullerenes, C$_{60}$) induce oxidative stress in the brain of juvenile largemouth bass *Environ. Health Perspect.* **112** 1058–62
[15] Isakovic A *et al* 2006 Distinct cytotoxic mechanisms of pristine versus hydroxylated fullerene *Toxicol. Sci.* **91** 173–83
[16] Yang X L, Huang C, Qiao X G, Yao L, Zhao D X and Tan X 2007 Photo-induced lipid peroxidation of erythrocyte membranes by a bis-methanophosphonate fullerene *Toxicol. In Vitro* **21** 1493–8
[17] Bosi S *et al* 2004 Hemolytic effects of water-soluble fullerene derivatives *J. Med. Chem.* **47** 6711–5
[18] Isakovic A *et al* 2006 Inactivation of nanocrystalline C$_{60}$ cytotoxicity by γ-irradiation *Biomaterials* **27** 5049–58
[19] Skals M, Jensen U B, Ousingsawat J, Kunzelmann K, Leipziger J and Praetorius H A 2010 Escherichia coli alpha-hemolysin triggers shrinkage of erythrocytes via K(Ca)3.1 and TMEM16A channels with subsequent phosphatidylserine exposure *J. Biol. Chem.* **285** 15557–65
[20] Belgorodsky B, Fadeev L, Kolsenik J and Gozin M 2006 Formation of a soluble stable complex between pristine C$_{60}$-fullerene and a native blood protein *Chembiochem* **7** 1783–9
[21] Markovic Z *et al* 2007 The mechanism of cell-damaging reactive oxygen generation by colloidal fullerenes *Biomaterials* **28** 5437–48
[22] Andrievsky G, Klochkov V and Derevyanchenko L 2005 Is the C$_{60}$ fullerene molecule toxic? *Fullerenes Nanotub. Carbon Nanostruct.* **13** 363–76
[23] Han S I, Kim Y S and Kim T H 2008 Role of apoptotic and necrotic cell death under physiologic conditions *BMB Rep.* **41** 1–10

[24] Berg C P *et al* 2001 Human mature red blood cells express caspase-3 and caspase-8, but are devoid of mitochondrial regulators of apoptosis *Cell Death Differ.* **8** 1197–206
[25] Bratosin D *et al* 2001 Programmed cell death in mature erythrocytes: a model for investigating death effector pathways operating in the absence of mitochondria *Cell Death Differ.* **8** 1143–56
[26] Lang K S *et al* 2003 Cation channels trigger apoptotic death of erythrocytes *Cell Death Differ.* **10** 249–56
[27] Matarrese P *et al* 2005 Peroxynitrite induces senescence and apoptosis of red blood cells through the activation of aspartyl and cysteinyl proteases *FASEB J.* **19** 416–8
[28] Harhaji L *et al* 2007 Multiple mechanisms underlying the anticancer action of nanocrystalline fullerene *Eur. J. Pharmacol.* **568** 89–98
[29] Vermes I, Haanen C and Reutelingsperger C 2000 Flow cytometry of apoptotic cell death *J. Immunol. Methods* **243** 167–90
[30] Deguchi S, Yamazaki T, Mukai S A, Usami R and Horikoshi K 2007 Stabilization of C_{60} nanoparticles by protein adsorption and its implications for toxicity studies *Chem. Res. Toxicol.* **20** 854–8
[31] Nikolic N *et al* 2009 Preparation and biodistribution of radiolabeled fullerene C_{60} nanocrystals *Nanotechnology* **20** 385102